Electron Spin-Echo Studies of the Copper Binding Site in Phenylalanine Hydroxylase from *Chromobacterium violaceum*

John McCracken,*[1a] Stephen Pember,[1b] Stephen J. Benkovic,[1b] Joseph J. Villafranca,[1b] Robert J. Miller,[1b] and Jack Peisach[1a]

Contribution from the Departments of Molecular Pharmacology and Physiology, Albert Einstein College of Medicine of Yeshiva University, Bronx, New York 10461, and Department of Chemistry, The Pennsylvania State University, University Park, Pennsylvania 16802.
Received May 8, 1987

Abstract: The active-site structure of the Cu(II)-containing phenylalanine hydroxylase from *Chromobacterium violaceum* was studied by electron spin-echo spectroscopy. Fourier transformation of the stimulated electron spin-echo envelope for the copper protein revealed frequency components characteristic of copper-histidyl imidazole coordination. The observed nuclear quadrupole frequencies at 0.55, 1.0, and 1.55 MHz are slightly different from those observed for model Cu(II)-imidazole complexes, 0.68, 0.72, and 1.40 MHz, but can be observed in Cu(II) complexes with 2-methylimidazole. A method of analysis by spectral simulation is presented for the quantitation of the number of equatorial imidazoles coordinated to Cu(II). In phenylalanine hydroxylase, two are bound.

Phenylalanine hydroxylase (PAH) (EC 1.14.16.1) catalyzes the conversion of phenylalanine to tyrosine. The reaction requires molecular oxygen and a tetrahydropterin cofactor that is oxidized to dihydropterin during substrate hydroxylation. The enzyme also requires a transition metal for activity. Mammalian PAH contains a single, tightly bound non-heme Fe(III) per monomer,[2] while PAH from *Chromobacterium violaceum* contains one Cu(II) per monomer.[3] Although these two enzymes contain different transition metals, both share similar mechanistic features. For example, the metal ions in both the mammalian and bacterial proteins must be reduced for enzymatic activity.[3,4] Although the function of the metal ion in the mechanism of the enzyme is not totally clear, data are supportive of the formation of a metal-peroxo species during the course of hydroxylation.[5,6] Participation of the metal in the actual transfer of oxygen to substrate has been suggested.[5] Additionally, the metal may also serve to activate the pterin molecule for initial reaction with molecular oxygen.[7]

PAH from *C. violaceum* is typical of many type II copper proteins containing a tetragonally coordinated Cu(II).[3] This protein is not highly colored, suggesting that it does not contain ligands contributing to a strong ligand-to-metal charge-transfer interaction.

Since the nature of the ligands, and their geometry, at the metal center in PAH is important for eventually understanding the reactivity of the metal ion, we have undertaken studies to determine their identity. In the current investigation we have used a pulsed EPR technique, electron spin-echo envelope modulation (ESEEM) spectroscopy,[8,9] to characterize the magnetic interactions between Cu(II) and weakly coupled magnetic nuclei (^1H and ^{14}N, in most protein samples) for the metal binding site.

Experimental Procedures

Materials. 6,7-Dimethyltetrahydropterin and 6-methyltetrahydropterin were prepared by the methods of Mager et al.[10] and Storm et al.,[11] respectively. Reduced pterin was prepared by catalytic hydrogenation over Pt/C. Catalase was purchased from Boehringer-Mannheim. Tris and Mes buffers, L-phenylalanine, and bovine serum albumin were obtained from Sigma. Dithiothreitol, for chemical recycling of dihydropterin during enzyme assays, was purchased from either Sigma or Aldrich.

Methods. Enzyme assays were performed on a Gilford 240 or 252 spectrophotometer, and pH measurements were made by a Radiometer 22 instrument equipped with a Model PHA 630-Pa scale expander and a Radiometer GK-2302C electrode.

Pulsed EPR Spectroscopy. The pulsed EPR spectrometer used in these studies has been described in detail elsewhere.[12] Two different microwave cavity systems were used for ESEEM measurements. For enzyme samples, a strip-line transmission cavity, identical with that developed by Mims,[13] was utilized. For model compound studies, a reflection cavity system that employs a folded strip line as the resonant element was used.[14,15] Both two-pulse (90°-τ-180°) and stimulated echo sequence (90°-τ-90°-T-90°) experiments were performed.[16] Typical measurement conditions were the following: microwave frequency, 9.0 GHz; magnetic field strength, 3100 G; microwave pulse power, 30 W; pulse width, 20 ns (full-width at half-maximum); sample temperature, 4.2 K; pulse repetition rate, 100 Hz. The τ values used to collect the stimulated ESEEM data presented below were set so that modulations due to weakly coupled protons were suppressed.[8]

Fourier transformation of the time domain data was performed on an LSI 11/73 based laboratory computer with the dead-time reconstruction technique of Mims.[17] Simulations of ESEEM data were also performed on the same computer by utilizing the matrix diagonalization procedures from the EISPACK library.[18]

Model Complexes. Copper(II) tetrakis(2-methylimidazole) was prepared by adding a 50-fold molar excess of recrystallized 2-methylimidazole to 2 mM copper(II) acetate in 50% v/v ethylene glycol/H_2O. The final pH was 7.3. The copper(II) diethylenetriamine 2-methylimidazole complex was prepared by adding 50 mM 2-methylimidazole to 5 mM copper(II) diethylenetriamine acetate in a 50% v/v ethylene glycol/H_2O solution, final pH 7.9.

Protein Purification. PAH from *C. violaceum* was purified by modification[19] of the procedure described by Nakata et al.[20] The protein

(1) (a) Albert Einstein College of Medicine. (b) The Pennsylvania State University.
(2) Gottschall, D.; Dietrich, R. F.; Benkovic, S. J.; Shiman, R. *J. Biol. Chem.* **1982**, *257*, 845-849.
(3) Pember, S. O.; Villafranca, J. J.; Benkovic, S. J. *Biochemistry* **1986**, *25*, 6611-6619.
(4) Wallick, D. W.; Bloom, L. M.; Gaffney, B. J.; Benkovic, S. J. *Biochemistry* **1984**, *23*, 1295-1302.
(5) Benkovic, S. J.; Lazarus, R. A. In *The Chemistry of Enzyme Action*; Mage, M. I., Ed.; Elsevier: New York, 1984; pp 373-388.
(6) Dix, T. A.; Bollag, G. A.; Domanico, P.; Benkovic, S. J. *Biochemistry* **1985**, *24*, 2955-2958.
(7) Pember, S. O.; Benkovic, S. J.; Villafranca, J. J.; Pasenkiewicz-Gerula, M.; Antholine, W. E. *Biochemistry* **1987**, *26*, 4477-4483.
(8) Mims, W. B.; Peisach, J. In *Biological Magnetic Resonance*; Berliner, L. J., Reuben, J., Eds.; Plenum: New York, 1981; Vol. 3, pp 213-264.
(9) Kevan, L. In *Time Domain Electron Spin Resonance*; Kevan, L., Schwartz, R. N., Eds.; Wiley-Interscience: New York, 1979; pp 279-342.
(10) Mager, H. I. X.; Addink, R.; Berends, W. *Recl. Trav. Chim. Pays-Bays* **1967**, *86*, 833-851.
(11) Storm, C. B.; Shiman, R.; Kaufman, S. *J. Org. Chem.* **1971**, *36*, 3925-3927.
(12) McCracken, J.; Peisach, J.; Dooley, D. M. *J. Am. Chem. Soc.* **1987**, *109*, 4064-4072.
(13) Mims, W. B. *Rev. Sci. Instrum.* **1974**, *45*, 1583-1591.
(14) Lin, C. P.; Bowman, M. K.; Norris, J. R. *J. Magn. Reson.* **1985**, *65*, 396-374.
(15) Britt, R. D.; Klein, M. P. *J. Magn. Reson.* **1987**, *74*, 535-540.
(16) Hahn, E. L. *Phys. Rev.* **1950**, *80*, 580-594.
(17) Mims, W. B. *J. Magn. Reson.* **1984**, *59*, 291-306.
(18) Smith, B. T.; Boyle, J. M.; Dongarra, J. J.; Garbow, B. S.; Ikebe, Y.; Klema, V. C.; Moler, C. B. In *Matrix Eigensystem Routines-EISPACK Guide*; Springer: New York, 1974; pp 19-22.

0002-7863/88/1510-1069$01.50/0

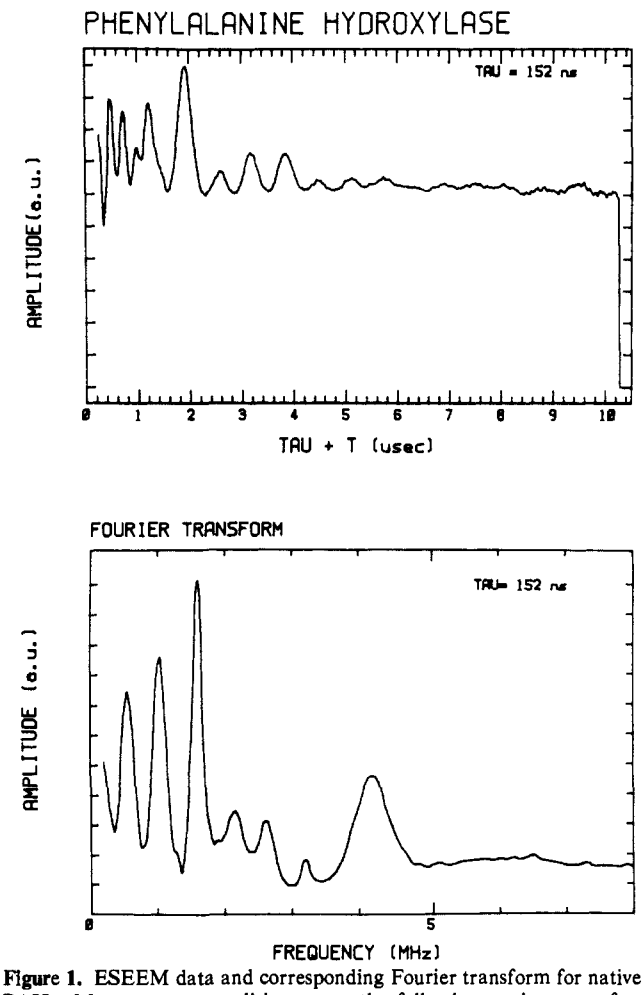

Figure 1. ESEEM data and corresponding Fourier transform for native PAH. Measurement conditions were the following: microwave frequency, 9.0210 GHz; magnetic field strength, 3100 G; microwave pulse power, 30 W; τ value, 152 ns; sample temperature, 4.2 K; pulse sequence repetition rate, 100 Hz; each time point, average of 80 events.

used in these studies had a specific activity of >12.0 units/mg and was ≅95% pure as determined by sodium dodecyl sulfate polyacrylamide gel electrophoresis and subsequent staining with coomassie blue. The concentration of enzyme used in electron spin–echo measurements was 630 μM.

Assays. The enzymatic activity of PAH with phenylalanine was measured from the change in absorbance at 275 nm, due to the formation of tyrosine (ϵ = 1.7 mM^{-1} cm^{-1}).[21] Specific details for the assay are given by Pember et al.[19] and Gottschall et al.,[2] respectively. Protein concentration was measured by the Lowry procedure.[22] When samples were in sulfonic acid buffers, the Bensadoun and Weinstein[23] modification was used.

Results and Discussion

A typical stimulated-echo ESEEM pattern for PAH together with its Fourier transform is shown in Figure 1. The spectrum shows four major frequency components, three narrow lines at 0.55, 1.0, and 1.55 MHz and a broad line centered at 4.1 MHz, as well as some weaker lines at 2.1, 2.6, and 3.1 MHz. These results are similar to those obtained by Mims and Peisach[24] for Cu(II)–imidazole model compounds. These authors demonstrated that ESE envelope modulations for these materials were due to magnetic coupling between Cu(II) and the remote ^{14}N of metal-coordinated imidazole, the coupling from directly coordinated, equatorially bound ^{14}N being too large to give rise to envelope modulation. The spectrum, obtained by Fourier transformation of the ESEEM pattern, consists of three narrow, low-frequency lines and a broad line at approximately 4 MHz and is a consequence of the Fermi contact interaction being approximately equal to twice the nuclear Zeeman frequency. Where the contact interaction is subtracted from the Zeeman interaction, the energy level splittings of the superhyperfine electron spin manifold are almost completely determined by the ^{14}N nuclear quadrupolar interaction. As the NQI is independent of magnetic field strength and direction, this manifold gives rise to the three sharp low-frequency lines, where the two lower frequencies add to give the third. The other electron spin manifold, where nuclear Zeeman and electron–nuclear hyperfine interactions are additive, gives rise to much broader spectral features. In this instance, where the ESEEM represents a powder pattern average, only the transition between the outermost levels is resolved. For Cu(II)–imidazole models studied near 3 kG, this transition occurs near 4 MHz (approximately $2\nu_n + a$, where ν_n is the nuclear Zeeman frequency and a represents the Fermi contact term).

The physical situation described above indicates that if measurements are made at a slightly higher microwave frequency and magnetic field strength (so that the effective g value remains constant), the frequencies of the three sharp lines will be virtually unaffected while the frequency of the broad component near 4 MHz should increase by twice the change in the nuclear Zeeman term. Such an experiment was performed on copper(II) tetrakis(imidazole) at a microwave frequency of 13.5 GHz. As the magnetic field for the measurement at $g_\perp$ was increased from 3.16 to 4.75 kG, the frequency of the broad component increased from 4.1 to 5.1 MHz, in agreement with the above prediction. For PAH, a similar frequency dependence on magnetic field strength was observed. Therefore, the quantum mechanical description by Mims and Peisach for Cu(II)–imidazole model complexes adequately describes the features of the PAH ESE spectrum and demonstrates that the remote ^{14}N from coordinated imidazole gives rise to the ESEEM data of Figure 1.

Another feature of the frequency spectrum for PAH shown in Figure 1 is the presence of three minor components at 2.1, 2.6, and 3.1 MHz. These peaks are narrow and are due to combination frequencies of the components at 0.55, 1.0, and 1.55 MHz, which are expected to appear when more than one nucleus with the same magnetic coupling gives rise to the ESEEM.[25-27] It is also possible that these minor components arise from nonlinearities in the detection system,[26] and this will be addressed below.

Although the ESEEM data for PAH are similar to those for the Cu(II)–imidazole complexes, they are not identical. For the Cu(II)–imidazole models, the narrow low-frequency components observed[24] are close to those obtained for protonated ^{14}N in imidazole and histidine powders, 0.68, 0.72, and 1.4 MHz, as studied by NQR.[28,29] It was this agreement between the ESEEM and NQR results that strengthened the analysis of Mims and Peisach and allowed for the identification of imidazole ligands in several copper proteins.[30,31] For PAH, these narrow low-frequency components are shifted to 0.55, 1.0, and 1.55 MHz, indicating that although the magnetic coupling between Cu(II) and the remote ^{14}N of bound imidazole is similar to that found for Cu(II)–imidazole model complexes, the NQI is different.

A similar shift in frequencies was found for other Cu(II) proteins as well: bovine plasma and porcine kidney amine oxidases[12] and galactose oxidase.[26] Explanations for these differences

(19) Pember, S. O.; Villafranca, J. J.; Benkovic, S. J. *Methods Enzymol.* **1987**, *142*, 50–56.
(20) Nakata, H.; Yamauchi, T.; Fujisawa, H. *J. Biol. Chem.* **1979**, *254*, 1829–1833.
(21) Miller, M. R.; McClure, D.; Shiman, R. *J. Biol. Chem.* **1975**, *250*, 1132–1140.
(22) Lowry, O. H.; Rosebrough, N. J.; Farr, A. L.; Randall, R. J. *J. Biol. Chem.* **1951**, *193*, 265–275.
(23) Bensadoun, A.; Weinstein, D. *Anal. Biochem.* **1976**, *70*, 241–250.
(24) Mims, W. B.; Peisach, J. *J. Chem. Phys.* **1978**, *69*, 4921–4930.
(25) Mims, W. B. *Phys. Rev. B: Solid State* **1972**, *5*, 2409–2419.
(26) Kosman, D. J.; Peisach, J.; Mims, W. B. *Biochemistry* **1980**, *19*, 1304–1308.
(27) Dikanov, S. A.; Shubin, A. A.; Parmon, V. N. *J. Magn. Reson.* **1981**, *42*, 474–487.
(28) Edmonds, D. T.; Summers, C. P. *J. Magn. Reson.* **1973**, *12*, 134–142.
(29) Hunt, M. J.; Mackay, A. L.; Edmonds, D. T. *Chem. Phys. Lett.* **1975**, *34*, 473–475.
(30) Mims, W. B.; Peisach, J. *J. Biol. Chem.* **1979**, *254*, 4321–4323.
(31) Mondovi, B.; Graziani, M. T.; Mims, W. B.; Oltzik, R.; Peisach, J. *Biochemistry* **1977**, *16*, 4198–4202.

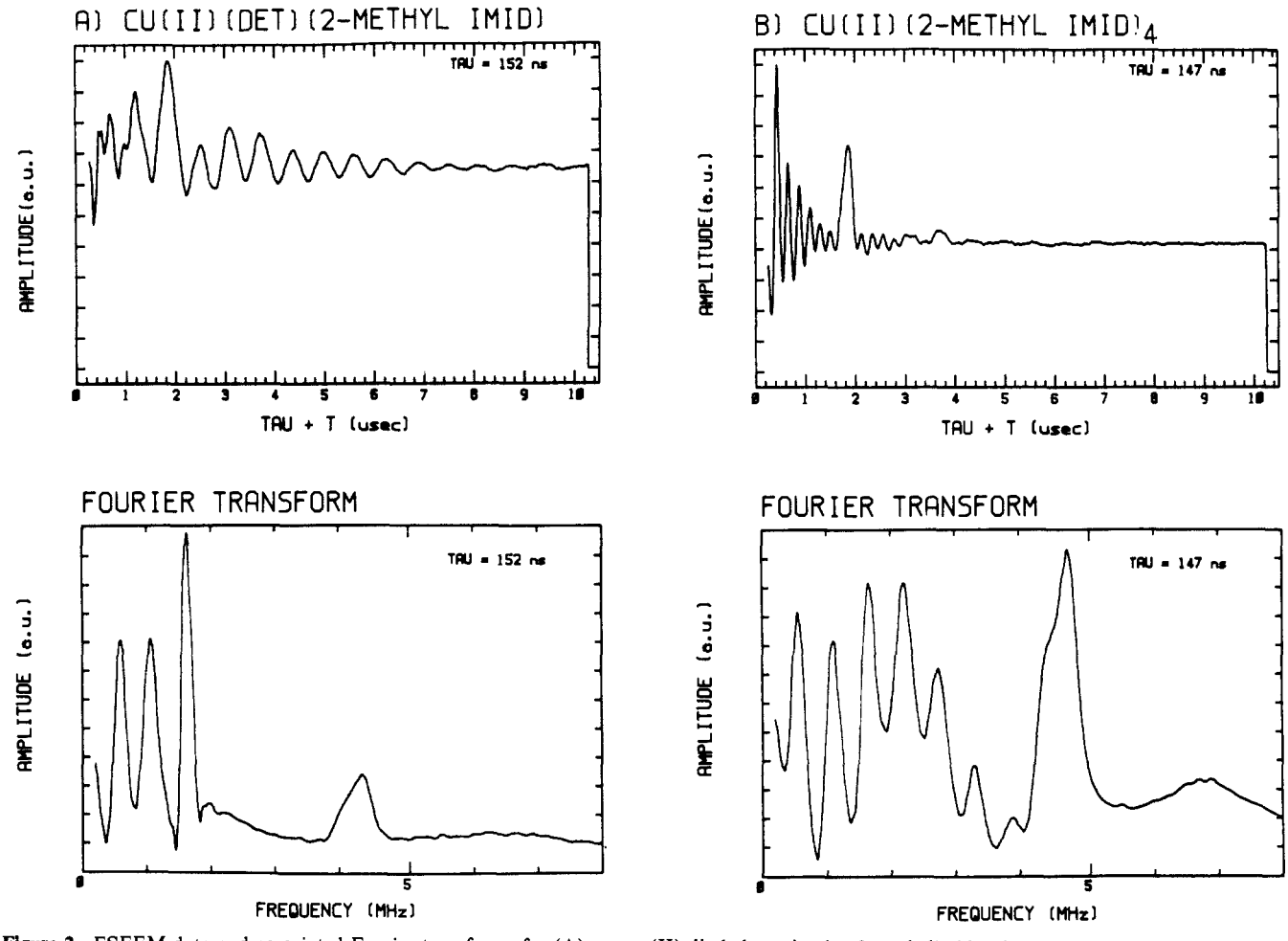

Figure 2. ESEEM data and associated Fourier transforms for (A) copper(II) diethylenetriamine 2-methylimidazole and (B) copper(II) tetrakis(2-methylimidazole). Measurement conditions for Figure 2A were the following: microwave frequency, 9.0248 GHz; pulse power, 30 W; magnetic field strength, 3100 G; τ value, 152 ns; sample temperature, 4.2 K. For Figure 2B, the measurement conditions were the following: microwave frequency, 9.0896 GHz; pulse power, 30 W; magnetic field strength, 3190 G; τ value, 147 ns; sample temperature, 4.2 K.

in the NQI parameters were given by Kosman et al.[26] These authors suggested that electronic perturbation of the imidazole ring or perturbation of the bond between the remote nitrogen and a hydrogen atom, possibly from a peptide hydrogen bond, might cause the observed differences in the NQI parameters by altering the electric field gradient and field gradient asymmetry about the remote ^{14}N nucleus. This view is supported by NQR measurements, where it was found that chemical substitution in the imidazole ring caused large changes in the electric field gradient asymmetry parameter, yet with minor changes in the magnitude of the electric field gradient.[29]

In order to determine the effect of structural modification in Cu(II)–imidazole complexes on the ESEEM, experiments were performed on two model compounds, copper(II) diethylenetriamine 2-methylimidazole and copper(II) tetrakis(2-methylimidazole). The numbering system for the imidazole is

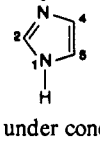

Stimulated echo data, taken under conditions similar to those used for PAH, along with their Fourier transforms are shown in Figure 2. For these models, narrow low-frequency components at 0.57, 1.03, and 1.6 MHz and a broad feature at 4.2 MHz are observed (Figure 2A). Thus, substitution of a methyl group at the 2-position in the imidazole ring causes a change in NQI parameters as compared to those found for Cu(II)–imidazole complexes and gives rise to a magnetic coupling between Cu(II) and ^{14}N similar to that found for Cu(II) in PAH. The cause for this change in the NQI may be due to differences in the electron-donating nature

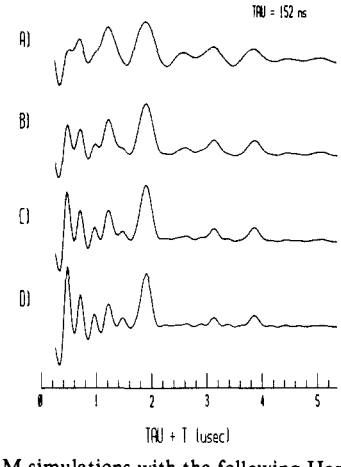

Figure 3. ESEEM simulations with the following Hamiltonian parameters: g_n, 0.403 49 (^{14}N); A_{xx}, 1.55 MHz; A_{yy}, 2.0 MHz; A_{zz}, 2.45 MHz (a = 2.0 MHz); e^2qQ, 1.68 MHz; η, 0.55; Euler angles, α = 23°, β = γ = 0°; H, 3100 G. Additional parameters used in the simulations were the following: τ, 152 ns; starting T, 120 ns; T increment, 10 ns; 512 time points computed. For Figure 3A only one ^{14}N contributes to the ESEEM, (B) two nitrogens, (C) three nitrogens, and (D) four nitrogens. Each simulation is multiplied by a single exponential decay function, $e^{-t/\tau}$, where τ was 2.5 μs.

of the methyl group and/or differences in ligand geometry, causing changes in the Cu(II)–imidazole bond orientations.[32] Experiments

(32) Freeman, H. C. In *The Biochemistry of Copper*; Peisach, J., Aisen, P., Blumberg, W. E., Eds.; Academic: New York, 1966; pp 77–115.

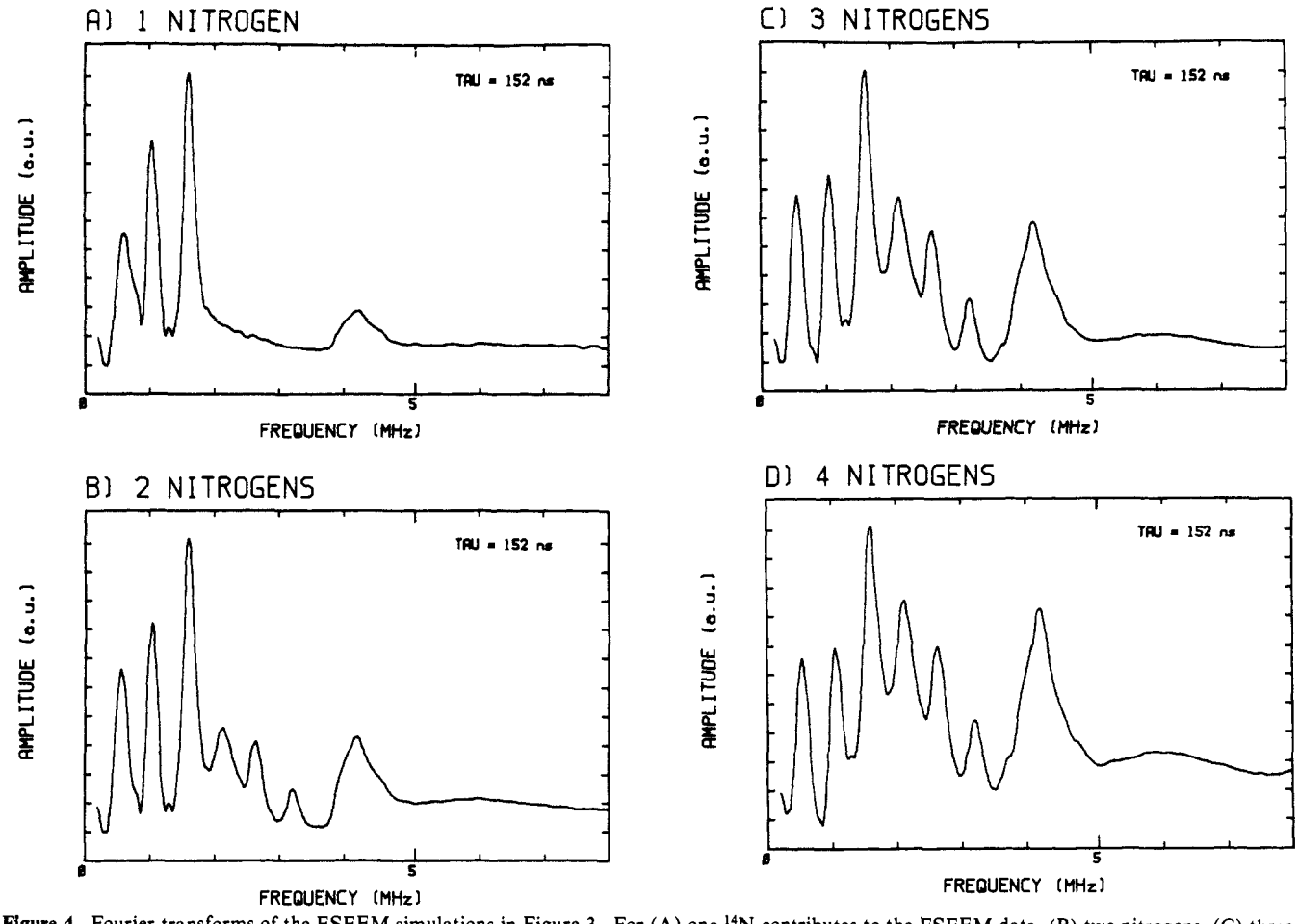

Figure 4. Fourier transforms of the ESEEM simulations in Figure 3. For (A) one ^{14}N contributes to the ESEEM data, (B) two nitrogens, (C) three nitrogens, and (D) four nitrogens.

aimed at sorting out the relative contribution of these factors are currently under way.

A comparison of the ESEEM data for copper(II) diethylenetriamine 2-methylimidazole (Figure 2A) and for copper(II) tetrakis(2-methylimidazole) (Figure 2B) shows that, as the number of nitrogens contributing to the modulation function increases from one to four, a number of spectral changes take place. The broad component at 4 MHz becomes more dominant in the modulation pattern, the combination frequencies at 2.1, 2.6, and 3.2 MHz that are not found with the single (2-methylimidazole) copper(II) model become large with the tetrakis(2-methylimidazole) model, and the apparent damping of the modulation function appears to increase. The failure to observe the combination frequencies for copper(II) diethylentriamine 2-methylimidazole is expected since only a single ^{14}N gives rise to the modulation in this case. This finding also indicates that the combination frequencies in the PAH spectrum are not artifacts but are due to the presence of more than one imidazole ligand bound to the copper (see footnote 2 in ref 26).

Because the frequency spectra for PAH and copper(II) 2-methylimidazole models are similar and the contribution of the combination frequencies in the spectrum for PAH (Figure 1) is much less prominent than that found for the copper(II) tetrakis(2-methylimidazole) model (Figure 2B), it is suggested that either two or three imidazole ligands are bound to Cu(II) in the protein. As one cannot easily differentiate from visual examination of the spectrum between two or three imidazole coordination to Cu(II), a detailed analysis of the three-pulse ESEEM data for PAH was undertaken to better characterize the magnetic coupling between Cu(II) and the remote ^{14}N of the histidyl imidazole ligands and to attempt to assess their number. This was achieved with the density matrix formalism developed by Mims,[25] with the Hamiltonian used to model the superhyperfine splittings for the ^{14}N ESEEM consisting of terms describing the nuclear Zeeman, electron–nuclear hyperfine, and nuclear quadrupolar interactions. Specific details concerning this analysis and its approximations have been given in recent publications.[12,33]

For the simulation of ESEEM data for PAH, the Euler angles that describe the relationship between the principle axis systems of the hyperfine and NQI tensors were initially set to zero, and e^2qQ and η were varied to account for the positions of the narrow, low-frequency components whose characteristics are primarily determined by this interaction. Then, the hyperfine tensor values were varied, with the Fermi contact portion ($a = {}^1/_3[A_{xx} + A_{yy} + A_{zz}]$) being adjusted to position the broad line at 4.1 MHz and the anisotropy in the tensor being used to predict the width and general shape of this line. Finally, the Euler angles that describe the relationship between the principle axis systems of the hyperfine and NQI tensors were varied to account for the relative contributions of the narrow, low-frequency components to the spectrum and the line shape of the 4.1-MHz component. It should be noted that this procedure is, in general, not as systematic as the above description implies, because the line shape of the frequency component at 4.1 MHz is dependent on both the characteristics of the hyperfine tensor and its orientation with respect to the NQI PAS. These features have been discussed in more detail by Reijerse and Keijzers.[34]

A parameter set that predicts the features of the PAH data is given in the legend to Figure 3. Here we show the simulated modulation functions using the parameter set at the τ value and magnetic field strength used in Figure 1 for the cases of (a) one ^{14}N, (b) two ^{14}N, (c) three ^{14}N, and (d) four ^{14}N. The simulations plotted in Figure 3B–D were obtained by the spherical model approximation[35] of the product rule for multiple magnetically

(33) Magliozzo, R. S.; McCracken, J.; Peisach, J. *Biochemistry* **1987**, *26*, 7923–7931.
(34) Reijerse, E. J.; Keijzers, C. P. *J. Magn. Reson.* **1987**, *71*, 83–96.

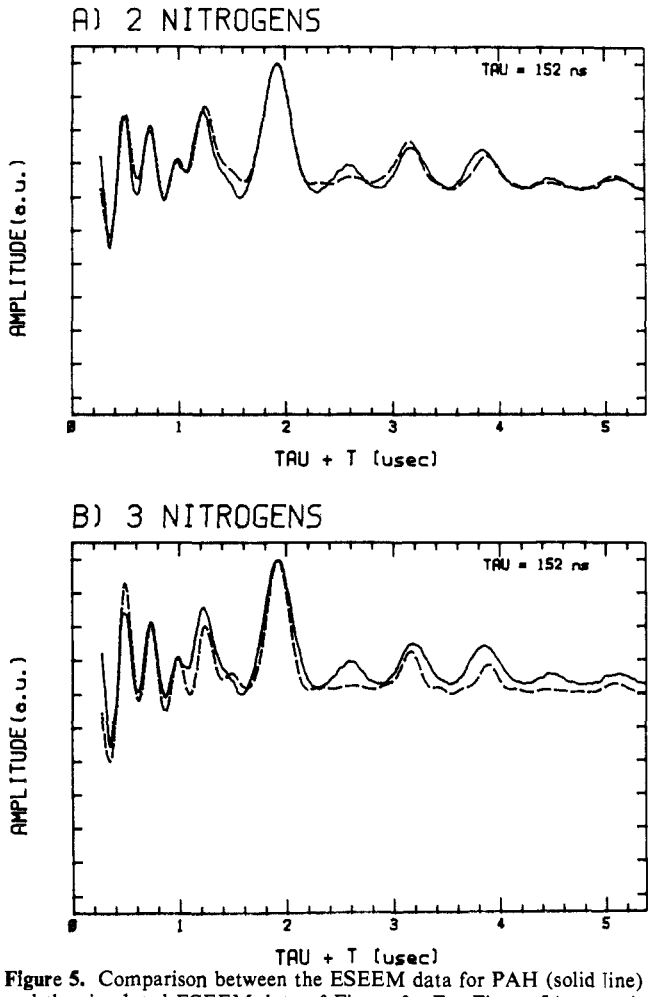

Figure 5. Comparison between the ESEEM data for PAH (solid line) and the simulated ESEEM data of Figure 3. For Figure 5A, two nitrogens contribute to the ESEEM, while for 5B three nitrogens contribute. Both experimental and theoretical waveforms are plotted on a scale that extends from zero echo amplitude to the maximum experimentally determined amplitude or theoretically predicted amplitude.

coupled nuclei.[36,37] The scales for all four simulations are different but have been arbitrarily adjusted for display purposes. Also, each simulation was multiplied by a single exponential decay function, $e^{-t/\tau}$, where τ = 2.5 μs, for aid in comparing these computed waveforms with the data.

Fourier transforms of the functions shown in Figure 3 are displayed in Figure 4 for the one ^{14}N through four ^{14}N cases. These simulations and Fourier transforms are in good agreement with the trends observed for the copper(II) 2-methylimidazole models. As one goes from a case where only one ^{14}N gives rise to the ESEEM to one where there are four ^{14}N's contributing, the relative contribution of the 4-MHz component to the data increases, along with the contributions of the combination frequencies at 2.1, 2.6, and 3.1 MHz. For a single ^{14}N nucleus, there are no combination frequences, and the three narrow, low-frequency components at 0.55, 1.0, and 1.55 MHz dominate the data. As the number of ^{14}N nuclei increases, the amplitudes of the combination frequencies increase and destructively interfere with the other low-frequency contributions to the ESEEM pattern, allowing the 4-MHz component to dominate the spectrum.

A comparison of the Fourier transforms of the simulated modulation functions (Figure 4) with that of PAH (Figure 1) indicates that two ^{14}N's give rise to the ESEEM. The criteria

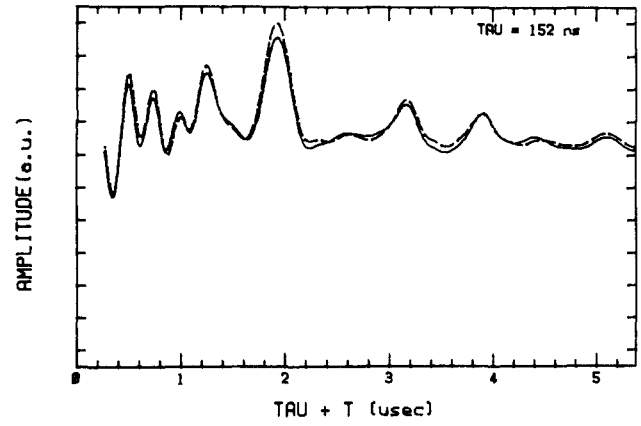

Figure 6. Comparison of ESEEM simulations for two ^{14}N nuclei coupled to Cu(II) by the product rule (solid line) and for the spherical model approximation to the product rule (dashed line). The magnetic coupling parameters used for both calculations are identical with those of Figure 3. The Euler angles describing the relative orientations of the hyperfine tensors for the two nuclei considered in the product rule formulation were the following: $\alpha = \beta = 90°$; $\gamma = 0°$. Both simulations were multiplied by a single exponential decay function, $e^{-t/\tau}$, where τ was 2.4 μs.

used in making this selection are the relative amplitudes of the combination frequency components and of the component at 4 MHz compared to those at 0.55, 1.0, and 1.55 MHz. A comparison of simulated modulation functions and depths with those obtained experimentally also bears this out and is shown in Figure 5. The solid lines are for the experimental data, while the dashed lines are simulations for (A) two-^{14}N and (B) three-^{14}N cases. The two-nitrogen simulation (Figure 5A) better accounts for the relative contributions of the various frequency components than the three-nitrogen model. This choice can be understood by examining the contributions of the 4-MHz component (periodicity 250 ns) to the ESEEM waveform for both the two- and three-^{14}N cases. For the two-^{14}N case, this component contributes very little to the time domain data after 1.5 μs, in good agreement with the PAH results. However, when three nitrogens are considered, the increased contribution from the combination frequencies gives rise to the interference effects described above, allowing the 250-ns periodicity to be more dominant in the ESEEM pattern. Therefore, in the three-nitrogen simulation (Figure 5B) one finds contributions from the 4-MHz component beyond 4 μs.

The agreement between experiment and theory (Figure 5A) is good considering that the calculations made use of the spherical model approximation to the product rule,[35-37] the simple form of the decay function used to compare experiment and theory, and the spherical integration over all possible orientations of the magnetic field direction with respect to the hyperfine tensor. The consequences of using the spherical model were checked by performing an exact calculation for two ^{14}N nuclei having identical magnetic coupling parameters but different coordinates with respect to the paramagnetic center. For this scheme, a second set of Euler angles is required to specify the relationship between the superhyperfine coupling tensors of the two nuclei, and one integrates the product of the computed modulation functions over the unit sphere. A comparison of the results of this procedure with those obtained by the spherical model (Figure 5A) are shown in Figure 6. The solid line represents the results for the proper usage of the product rule where the principle axis of the hyperfine tensor for the second nucleus is 90° from that of the first. The hyperfine and NQI parameters are the same for both nuclei, and the same decay function was used for both simulations. The differences between these two predictions and those of the other orientations examined are minor and would be difficult to distinguish experimentally. The reason for the validity of the spherical model in this instance probably stems from the ESEEM being dominated primarily by the NQI, which is independent of magnetic field direction. It should be noted that this approximation will not be valid in all cases. For instance, Dikanov and co-workers[36] found that, for a small number of magnetically

(35) Kevan, L.; Bowman, M. K.; Narayana, P. A.; Boeckman, R. K.; Yudanov, V. F.; Tsvetkov, Yu. D. *J. Chem. Phys.* **1975**, *63*, 409-416.
(36) Dikanov, S. A.; Yudanov, V. F.; Tsvetkov, Yu. D. *J. Struct. Chem. (Engl. Transl.)* **1977**, *18*, 460-476.
(37) Mims, W. B.; Davis, J. L. *J. Chem. Phys.* **1976**, *64*, 4836-4846.

coupled deuterons, the ESEEM patterns predicted by the spherical model approximation were much different from those obtained by the product rule when the superhyperfine splittings were dominated by the hyperfine interaction.

In a separate study, the consequences of spherical integration at $g_\perp$ in the PAH spectrum were examined in more detail with the angle selection scheme described by Hurst et al.[38] From the **g** tensor and Cu(II) nuclear hyperfine tensor values determined for PAH,[7] it can be shown that transitions from all four Cu(II) nuclear hyperfine levels contribute to the ESEEM under the conditions used for our measurements. Therefore, the spherical averaging scheme would be replaced in the ESEEM calculation by four line integrals. It was found that this model predicts the three narrow, low-frequency components with the same NQI parameters used in our simulations (Figure 3). However, three additional sharp lines at approximately 1, 3, and 4 MHz were also predicted for the other electron-spin manifold. As these additional components were not observed for the protein or for the copper(II) diethylenetriamine 2-methylimidazole model and the wide line width of the 4.1-MHz component is not accounted for by the angle selection scheme, it is concluded that a full spherical average is probably more appropriate for the treatment of the data at $g_\perp$. It is possible that some combination of cross-relaxation processes[39] together with effects due to Cu(II) isotopic mixture, Cu(II) nuclear quadrupole interactions, and the narrow microwave pulses required for ESEEM serve to broaden out the line integrals predicted by the angle-selection approach to the extent that a spherical average is warranted.

The ESEEM results for PAH do not exclude the possibility that there are additional ^{14}N-containing ligands bound to Cu(II). As mentioned above, Cu(II) model compound studies have shown that equatorially bound, directly coordinated ^{14}N does not give rise to ESEEM at *X*-band. Examples of this are the directly coordinated ^{14}N in Cu(II)–imidazole model complexes[24] and the equatorially bound amino nitrogens in copper(II) glycylglycine and copper(II) tetrakis(methylamine).[40] Whereas ESEEM's arising from imidazole equatorially coordinated to Cu(II) are due to electron–nuclear interactions between the electron spin of the Cu(II) and the remote, noncoordinated ^{14}N of the ligand,[24] axially coordinated imidazole, as found in Cu(II)-substituted myoglobin,[41] gives rise to modulations from the directly coordinated ^{14}N. Similar couplings are observed for a copper(II) bis(benzacetoacetonate) complex with pyridine axially coordinated to the metal ion.[42] The modulation depths in both axial ^{14}N complexes are shallow (<10% of the echo amplitude at *X*-band) as compared to those observed for the remote ^{14}N of equatorially coordinated imidazole. From a theoretical treatment of ^{14}N modulation data for PAH and for the axially bound ^{14}N complexes cited above, it can be shown that the modulations from an axial ^{14}N would be masked by ESEEM from two imidazoles equatorially coordinated to Cu(II), as we have shown to occur in PAH. Therefore, we cannot rule out the possibility that an axial ^{14}N-containing ligand is bound to Cu(II) in *C. violaceum* PAH.

In summary, ESEEM studies have allowed the assignment of imidazole as a ligand to Cu(II) in PAH from *C. violaceum*. The observations of minor-frequency components attributable to combinations of ^{14}N superhyperfine frequencies arising from the remote nitrogen of equatorially bound imidazole indicate that more than one such ligand is bound. This conclusion was strengthened by an ESEEM study of copper(II) 2-methylimidazole model compounds and computer simulations of the protein ESEEM data, based on the theoretical model of Mims,[25] which indicates that two imidazoles are bound equatorially to Cu(II).

Abbreviations

PAH, phenylalanine hydroxylase; EPR, electron paramagnetic resonance; Mes, 2-*N*-morpholinoethanesulfonic acid; Tris, tris(hydroxymethyl)aminomethane; ESEEM, electron spin–echo envelope modulation; ESE, electron spin–echo; NQI, nuclear quadrupole interaction; NQR, nuclear quadrupole resonance; PAS, principle axis system.

Acknowledgment. This work was supported by NSF Grants PCM8103670 and PCM8409737 (S.J.B.) and NIH Grants GM29139 (J.J.V.) and RR02583 and HL13399 (J.P.).

(38) Hurst, G. C.; Henderson, T. A.; Kreilick, R. W. *J. Am. Chem. Soc.* **1985**, *107*, 7294–7299.
(39) Dalton, L. R.; Kwiram, A. L. *J. Chem. Phys.* **1972**, *57*, 1132–1145.
(40) Mims, W. B.; Peisach, J.; Davis, J. L. *J. Chem. Phys.* **1977**, *66*, 5536–5550.
(41) Rifkind, J.; McCracken, J.; Peisach, J., unpublished results.
(42) Cornelius, J.; McCracken, J.; Belford, R. L.; Peisach, J., unpublished results.